Periodic and chaotic output pulsations in a single-mode inhomogeneously broadened laser

M. F. H. Tarroja and N. B. Abraham
Department of Physics, Bryn Mawr College, Bryn Mawr, Pennsylvania 19010

D. K. Bandy and L. M. Narducci
Department of Physics and Atmospheric Science, Drexel University, Philadelphia, Pennsylvania 19104
(Received 19 May 1986)

We compare the results of theoretical and experimental studies of a unidirectional, single-mode, inhomogeneously broadened ring laser. We find reasonable qualitative agreement between the calculated and observed output pulsations under resonant and detuned operating conditions, and over a fairly wide range of the pump parameter. With the help of homodyne and heterodyne power spectra, we find that the periodic output field oscillations are usually asymmetric in the phase plane. Over restricted regions of the control parameter space, on the other hand, both symmetric and asymmetric pulsations are found, sometimes coexisting for the same parameter values. The power spectra and temporal oscillations often resemble results from the Lorenz model for a single-mode homogeneously broadened laser.

I. INTRODUCTION

Inhomogeneously broadened lasers are not often considered simple systems. Spectral holeburning and Doppler effects are often considered sources of extraordinary complexity. We find that, nevertheless, the inhomogeneously broadened laser offers a dynamical system which can be studied successfully theoretically by analytical and numerical techniques.

Theoretical studies of the conceptually simpler system, the homogeneously broadened ring lasers, have found both instabilities and regular and chaotic pulsations. These results were first found in studies by Oraevskii, Uspenskii and co-workers,[1] extended by Haken,[2] Risken and Nummedal,[3] and Graham and Haken,[3] and elaborated upon by several others in more recent times.[4] However, attempts to observe these instabilities in laboratory systems have been limited, in part because of the stringent requirements imposed on the laser parameters and perhaps also because of the role of the transverse field variations[5] whose dynamical significance is still very poorly understood.

Experimental progress is being made, however. Klische and Weiss[6] have recently reported the observation of unstable and chaotic behavior in a far-infrared NH_3 laser with a narrow homogeneously broadened atomic profile and high unsaturated gain; almost at the same time, Narducci and collaborators[7] discovered the existence of stable periodic solutions in a single-mode model of a homogeneously broadened laser. Their results offer additional support to the claim[6] that the NH_3-laser experiments represent a close realization of the physical requirements for the observation of single-mode instabilities in this type of laser system.

In spite of the success of Weiss's work, many other homogeneously broadened single-mode lasers offer a puzzling array of pulsations. CO_2 and semiconductor lasers, for example, display time-dependent forms of behavior that cannot easily be explained by the available theoretical models. In addition, there are also unexplained pulsations of some of the earliest homogeneously broadened laser systems, e.g., the solid-state ruby and YAG lasers (where YAG denotes yttrium aluminum garnet).

In contrast with results for homogeneously broadened lasers, many effects in the inhomogeneously broadened lasers seem more understandable. In 1973, Idiatulin and Uspenskii[8] proposed a simplified theoretical model for inhomogeneously broadened laser systems (using two groups of atoms with different resonant frequencies) which showed that even this approximate representation of inhomogeneous broadening dramatically altered the behavior of laser instabilities. In particular, they showed that in their model there was a marked reduction of the threshold for the onset of pulsations, a feature also found in later, more systematic investigations of inhomogeneous broadening. Casperson's discovery[9] of coherent pulsations in a cw-excited, low-pressure xenon laser and his subsequent theoretical investigations[9–11] stimulated a resurgence of interest in this area, opening the way to new and significant experimental developments[12,13] and putting the existing models[14] in the position to provide some guidelines for a systematic organization of the data.

The work on inhomogeneously broadened lasers presented in this paper has both theoretical and experimental components. It is carried out in the same spirit as Casperson's analysis in Ref. 10 and both corroborates and complements many of his findings. Our theoretical studies are based on the plane-wave Maxwell-Bloch (MB) equations for an inhomogeneously broadened, single-mode ring laser. This is the same model that was studied by Lugiato and collaborators[15] in their analyses of the steady state and their stability properties and by Bandy and collaborators[16] in connection with the time-dependent behavior. The experiments reported in this paper involve a single-mode ring laser where the gas pressure can be changed to adjust the degree of inhomogeneous broadening.

The aim of this work is to test the reliability of the

 ©1986 The American Physical Society

plane-wave MB model by direct comparison of its numerical predictions with observations of the output of a Xe-He unidirectional ring laser. Previous studies of the theoretical model have focused on the determination of instability threshold conditions and on the observation of time-dependent intensity pulsations and their corresponding homodyne spectra. We now consider numerical results for parameter values that are consistent with the experimental conditions, and calculate the spectrum of the electric field of the unstable laser by a heterodyne technique. Heterodyne spectroscopy has long been used experimentally. Here we show that in addition to providing a basis for systematic comparison of theory and experiment, heterodyne spectra can remove ambiguities in the interpretation of the Fourier transform of the intensity. The intensity spectra (or homodyne spectra) cannot distinguish between symmetry-breaking transitions and period-doubling bifurcations. We also use phase-space portraits for further clarification of these types of transitions.

In Sec. II we review the semiclassical MB equations for the ring laser and summarize a few relevant facts on their steady states and stability properties. In Sec. III we review the Xe-He laser system and related instrumentation, and provide a list of the relevant experimental parameters and their theoretical counterparts. We present our experimental data and the results of numerical simulations in Sec. IV, and our conclusions and a discussion of the results in Sec. V.

II. A REVIEW OF THE MODEL

The laser is modeled as a collection of active two-level systems in an unidirectional ring cavity that operates in a single-mode configuration. The gain profile of the active medium is inhomogeneously broadened with a Gaussian distribution

$$g(\tilde{\delta})=(2\pi\tilde{\sigma}_D^2)^{-1/2}\exp(-\tilde{\delta}^2/2\tilde{\sigma}_D^2) \tag{2.1}$$

around the center of the atomic transition, ω_A. The half width at half maximum is $\sqrt{2\ln 2}\tilde{\sigma}_D$; both the running frequency variable $\tilde{\delta}$ and $\tilde{\sigma}_D$ are scaled to $\gamma_\perp$, the half-width of each homogeneously broadened atomic component.

With reference to the carrier frequency ω_L of the laser, the basic equations of motion for the slowly varying field and atomic variables are[17]

$$(d/d\tau)X(\tau)=-\tilde{\kappa}\{[1-i(\tilde{\phi}/\tilde{\kappa})]X(\tau)+2C\int d\tilde{\delta}g(\tilde{\delta})P(\tilde{\delta},\tau)\}\ , \tag{2.2a}$$

$$(d/d\tau)P(\tilde{\delta},\tau)=X(\tau)D(\tilde{\delta},\tau)+[1+i(\tilde{\Delta}+\tilde{\delta})]P(\tilde{\delta},\tau)\ , \tag{2.2b}$$

$$(d/d\tau)D(\tilde{\delta},\tau)=-\tilde{\gamma}\{(\tfrac{1}{2})[X^*P(\tilde{\delta},\tau)+XP^*(\tilde{\delta},\tau)]+D(\tilde{\delta},\tau)+1\}\ , \tag{2.2c}$$

where $\tilde{\phi}$ is the offset between the laser carrier and the empty cavity mode in units of $\gamma_\perp$; $\tilde{\Delta}$ is the displacement of the center of the atomic line, $(\omega_A-\omega_L)/\gamma_\perp$; and $\tilde{\gamma}=\gamma_\parallel/\gamma_\perp$ denotes the ratio of the population and polarization relaxation rates. The variables $P(\tilde{\delta},\tau)$ and $D(\tilde{\delta},\tau)$ label the polarization and population difference, respectively, of the atomic packet located at a frequency $\tilde{\delta}$ from the center of the gain line; $X(\tau)$ denotes the slowly varying amplitude of the cavity field scaled to the square root of the saturation intensity and τ is equal to $\gamma_\perp t$. Variables and decay rates capped by a tilde are measured in units of $\gamma_\perp$.

For selected values of the cavity and atomic decay rates, the excitation parameter C and the inhomogeneous width $\tilde{\sigma}_D$, the state equation of the single-mode laser can be single or multivalued and the stability of each steady state can be analyzed as shown in Ref. 18. Usually, a multivalued state equation develops only for relatively large values of the detuning and high excitation. In our present studies we will work in the single-valued domain.

The temporal evolution of the system could be calculated using as initial conditions either a slightly perturbed stationary state or the long-term values of the variables from a simulation corresponding to a slightly different control parameter. Using the latter procedure and small changes in one parameter we obtain a reasonable simulation of the slow parameter scans that are used in many experiments. In order to keep to a minimum the trivial time evolution due to shifts in the optical carrier frequency, each time the equations were restarted for new parameter values, the carrier wave frequency was reset to the frequency of the steady-state solution for those parameter values. Nevertheless, the time-dependent solutions for the slowly varying amplitudes often revealed additional frequency shifts induced by the dynamical pulsations.

As a prelude to the analysis of time-dependent solutions, we now review some relevant steady-state and linear stability results. Figure 1 shows the modulus of the steady state solution of the field, $|X_{st}|$, as a function of the gain parameter C for resonant operations. The state equation is independent of $\tilde{\gamma}$ and is single valued for the parameters used in these simulations. The eigenvalues of the linear stability analysis depend on $\tilde{\gamma}$. However, in the experiments reported here, this parameter is held virtually

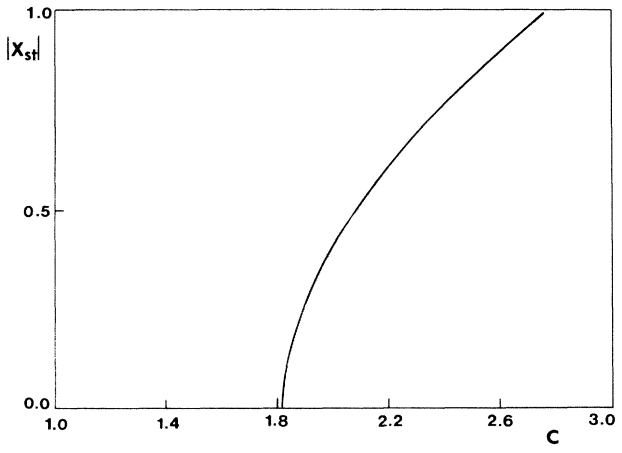

FIG. 1. Steady-state modulus of the field amplitude $|X_{st}|$ for a Gaussian-broadened laser in resonance as a function of the gain parameter C for $\tilde{\sigma}_D=3.72$, $\tilde{\kappa}=4.67$, and $\tilde{\gamma}=0.183$.

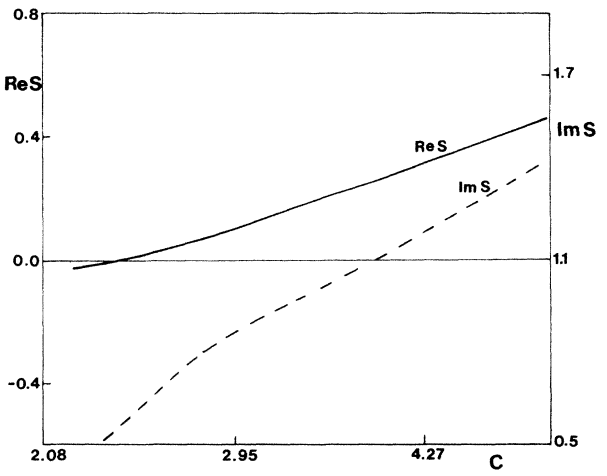

FIG. 2. Real part (solid line) and the imaginary part (dashed line) of the two most unstable eigenvalues of the secular equation as functions of C for parameters used in Fig. 1.

constant by using the same pressure mixtures of gases. Hence, in Fig. 2 we show only a typical result for the two most unstable eigenvalues.

The first laser threshold, as shown in Fig. 1, occurs for a value of the gain parameter $C=1.82$. The onset of unstable behavior occurs at $C=2.36$ as shown in Fig. 2. This instability is a Hopf bifurcation as evidenced by the finite imaginary parts of the eigenvalues whose real parts vanish at the bifurcation threshold. The imaginary part of these eigenvalues is a good estimator of the pulsation frequency in the early stages of the evolution of the system from the unstable steady state. This relation is more exact if just above the instability threshold there are only small amplitude limit cycles about the unstable steady state. Often in practice it is also a good approximation even well into the regime of large pulses.

III. EXPERIMENTAL CONFIGURATION

The He-Xe laser used in this experiment is shown schematically in Fig. 3; it consists of two gas discharge tubes of lengths 11 cm and 19 cm, respectively, filled with known and controllable amounts of ^{136}Xe (99% isotopic purity) and He gases, and four reflectors, three of which have 99% reflectivity, while the last has a reflectivity of 90%. The laser operates as an unidirectional device with the help of two 45° Faraday rotators (FR) and two wire-grid linear polarizers (P). The 2-mm-diameter discharge tubes and their Brewster's angle quartz windows along with the range of currents and pressures selected suppress all laser lines of the xenon gas except for the 3.51-μm line. The total cavity length of 0.753 m sets the spacing between successive empty-cavity longitudinal modes large enough that only one mode at a time falls within the 100-MHz Doppler-broadened gain profile of the active medium for the range of excitations used. All of the various losses in the cavity can be simulated by an effective reflectivity parameter $R\approx 0.372$ corresponding to $\tilde{\kappa}\approx 5$.

The output signal from the laser is divided into two parts. One part is chopped at a frequency of 500 Hz and

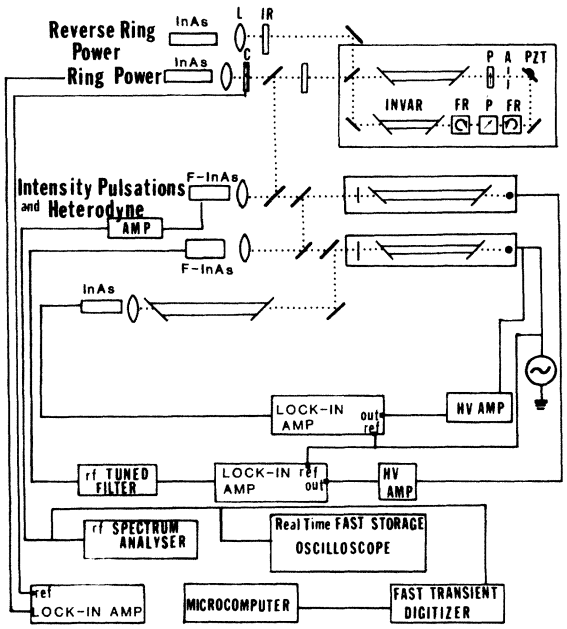

FIG. 3. Setup of the optics and electrons for a unidirectional ring laser: P, wire-grid polarizer; FR, Faraday rotator; A, aperture; F-InAs, high-speed photodiode; InAs, low-speed photodiode; C, chopper; L, quartz lens; IR, 3.5-μm dielectric filter; PZT, piezoelectric mirror translator.

detected by a 1-mm-diameter InAs photodiode. The output of the photodiode is fed into a lock-in amplifier for the measurement of the average power output. The other part of the output signal is mixed with a reference beam from a single-frequency Fabry-Perot laser which is stabilized through a separate feedback loop. (The stabilization circuit involves a second modulated Fabry-Perot laser which is stabilized to the peak of the gain of a reference amplifier.) The resulting beat signal is focused by a lens onto a 0.01-mm^2 reverse-biased InAs photodiode whose high-speed response, within a range 1 kHz—100 MHz, allows the detection of both the intensity fluctuations of the ring laser and the interlaser beat signals. The output from the photodiode is amplified and sent to a fast storage oscilloscope, for a display of the intensity pulsations, and to a radio-frequency spectrum analyzer that shows simultaneously the homodyne spectrum of the output intensity of the ring laser (at the low end of the frequency scale) and the heterodyne spectrum of the interlaser beat frequencies (at the high-frequency end of the 100-MHz display). We have recorded the shapes of the homodyne and heterodyne spectra and the position of the relevant peaks as functions of the excitation current for a fixed value of the cavity detuning. Similarly, we followed the behavior of the spectral features for fixed values of the current as the detuning was varied continuously.

IV. REVIEW OF DATA AND THEORETICAL SIMULATIONS

We now examine the numerical results of the model using the values of the parameters appropriate to our experiments which are listed in Table I. These results are ob-

TABLE I. Values of the parameters to be used for theoretical comparisons for the two experimental conditions studied.

Pressure	$\gamma_\perp$ (10^6 s^{-1})	$\tilde{\sigma}_D$	$\tilde{\kappa}$	$\tilde{\gamma}$
1 Torr of He 172 mTorr of Xe	78.8±3.5	3.72±1.0	4.67	0.183
667 mTorr of He 175 mTorr of Xe	59.4±2.8	4.93±1.5	6.19	0.243

tained by numerical integration of Eqs. (2.2) using a fourth-order Runge-Kutta scheme and an extended trapezoidal rule for the evaluation of the frequency integral. (For further information, see Ref. 15.) A fast-Fourier-transform routine decomposes the output intensity into its frequency components and calculates the associated power spectrum. This technique, referred to as homodyne spectral analysis, is a widely used diagnostic tool for the observation of subharmonic bifurcations and the appearance of incommensurate frequencies. A common difficulty of this method is its inability to distinguish between symmetry-breaking transitions and period-doubling bifurcations. In order to correct this problem we simulate the heterodyne beating of the output field with a reference source by superimposing the calculated field of interest with a reference optical wave having a fixed amplitude and carrier frequency. The total calculated intensity is Fourier analyzed using a fast-Fourier-transform routine. The heterodyne spectra of the time-dependent solutions show a clearer picture of the bifurcations. For a complete description of this procedure, see Appendix B of Ref. 19.

Figure 4 provides a summary of the dynamical behavior of the system under resonant conditions by overlaying the appropriate steady-state curve for the modulus of the output field with a set of symbols and ranges denot-

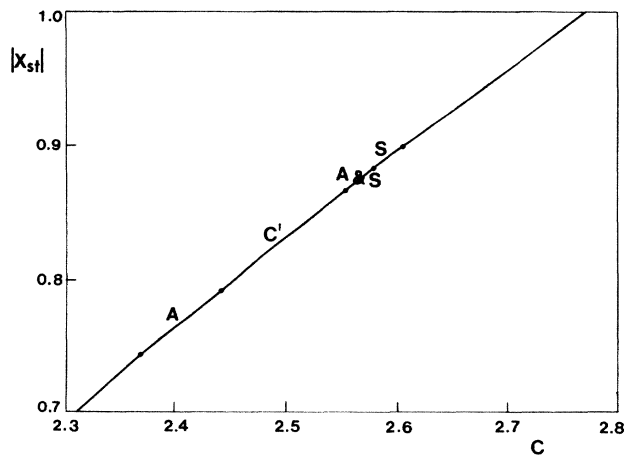

FIG. 4. Expanded region of the steady-state curve in Fig. 1. *A*, asymmetric attractor; *C'*, chaotic attractor; *S*, symmetric attractor; *A&S*, region of coexistence of both asymmetric and symmetric attractors.

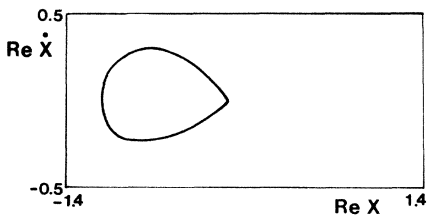

FIG. 5. Projection of the phase-space trajectory in the (ReX,Re$\dot{X}$) plane, using $C=2.3677\ldots$ ($|X_{st}|=0.79$) and the governing parameters of Fig. 1. A strongly asymmetric attractor is revealed.

ing the different types of output oscillations. For values of the gain just above the instability threshold, the laser intensity shows weak oscillations about its mean value. The heterodyne spectrum shows that there are weak sidebands equally spaced about a strong spectral component corresponding to a nonzero mean value at the steady-state laser frequency. A solution of this type, characterized by a strong average component, is called asymmetric because of the asymmetry in its plot in the phase space Re$\dot{X}$ versus ReX and is labeled by A in the figure. In this particular case, the small amplitude limit cycle indicates that the initial instability develops as a supercritical (or forward) Hopf bifurcation.

With increasing gain, the asymmetric pulsations become stronger, corresponding to a larger limit cycle revealed by a single large loop in the phase space, as shown in Fig. 5. As the gain is further increased, the calculated output field develops broadband spectral features with some distinguishable peaks and eventually evolves into a more fully chaotic solution (labeled C' in Fig. 4). Within the region labeled C', we observe windows of symmetric, period-1 solutions, first evidence that both symmetric and asymmetric attractors are present in this system.

Upon increasing the gain further, the chaotic region is followed by a region of weak asymmetric periodic solutions of the type shown in Fig. 6. The nature of this phase portrait is quite different from that of the characteristic limit cycle near threshold and suggests that the asymmetric features of the attractor are becoming weaker. Evidence of this behavior is also offered by the initially strong central component observed in the heterodyne spectra that weakens upon emerging from the chaotic region and eventually disappears in a smooth transition to

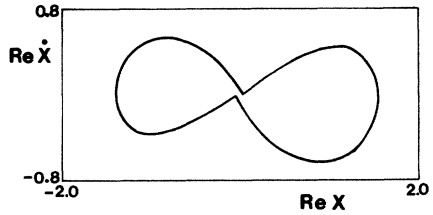

FIG. 6. Projection of the phase-space trajectory in the (ReX,Re$\dot{X}$) plane, using $C=2.566\,22\ldots$ ($|X_{st}|=0.875$) and the governing parameters of Fig. 1. A weakly asymmetric attractor is revealed.

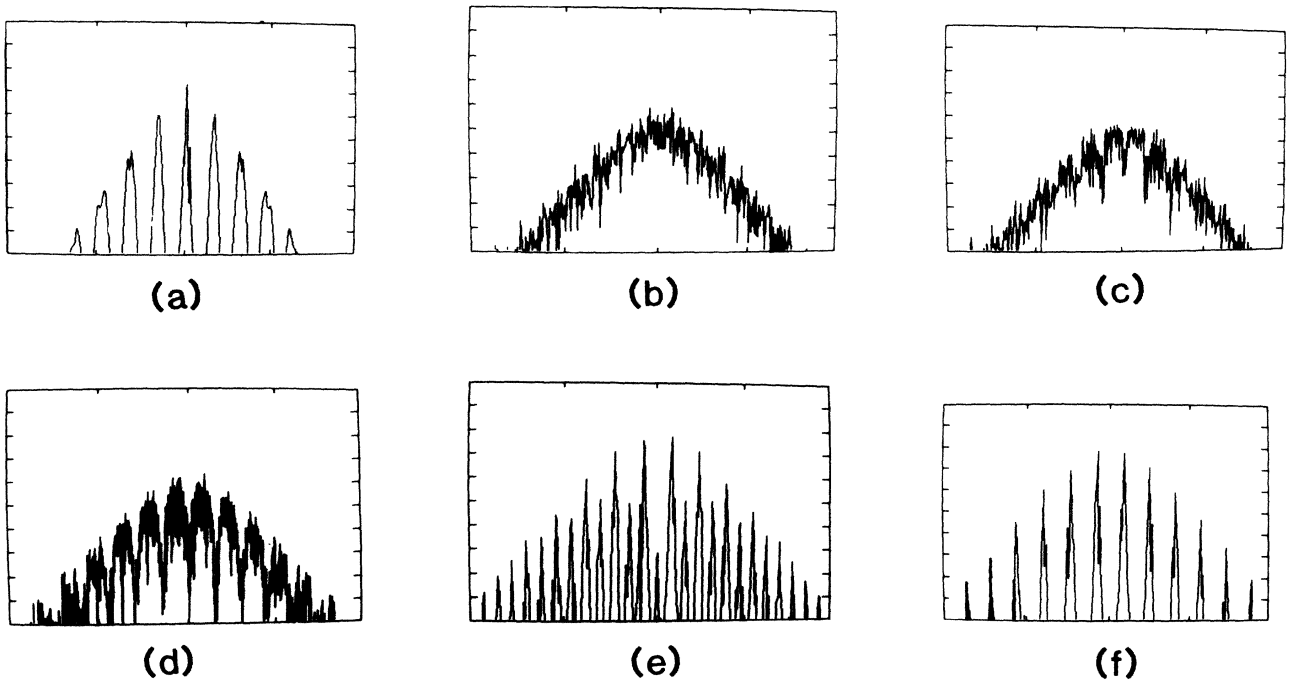

FIG. 7. Numerically obtained heterodyne power spectra with cavity tuned to resonance for parameters corresponding to pressure conditions in Fig. 1. Spectra are shown as the excitation increases from (a) to (f). A unit on the horizontal axis corresponds to 37.6 MHz and a unit on the vertical axis corresponds to 6.5 dB.

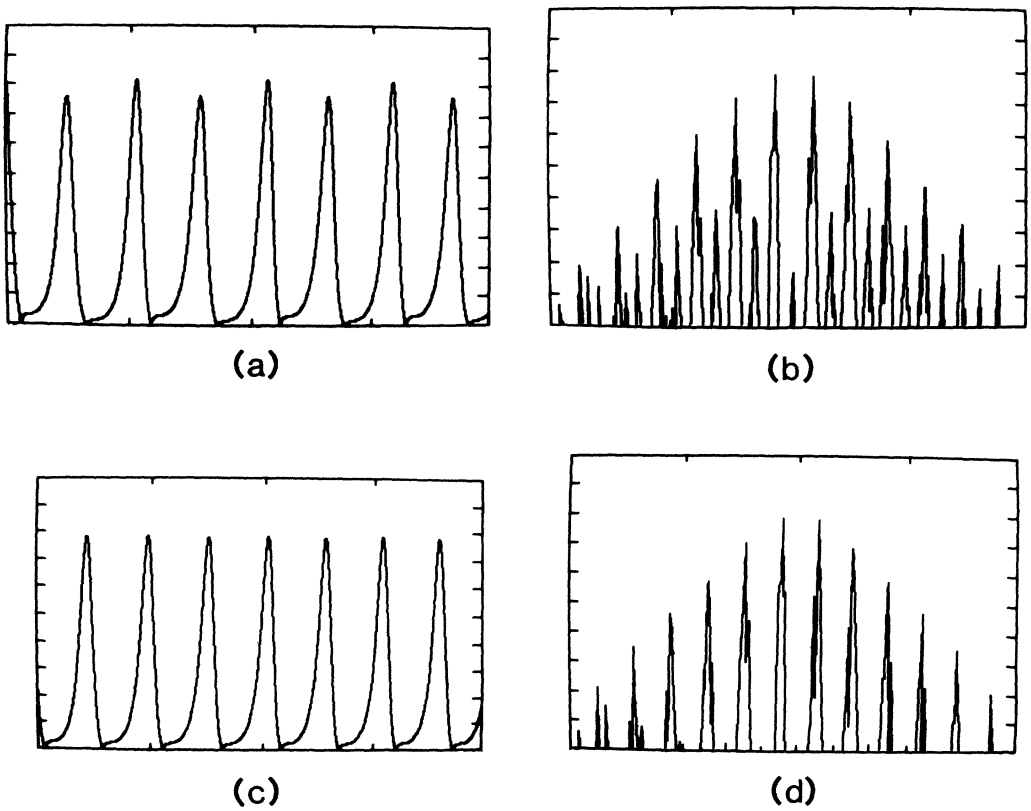

FIG. 8. (a) Numerically generated time dependence of the electric field amplitude for $C=2.574\,14\ldots$ ($|X_{st}|=0.88$) and parameters used in Fig. 1. Example of an asymmetric solution in the region of coexisting attractors. (b) Heterodyne spectrum of the asymmetric solution of (a). (c) Numerically generated time dependence of the electric field amplitude for $C=2.574\,14\ldots$ ($|X_{st}|=0.88$) and parameters used in Fig. 1. Example of a symmetric solution in the region of coexisting attractors. (d) Heterodyne spectrum of the symmetric solution of (c).

the symmetric solution (labeled S in Fig. 4).

An important aspect of this gain scan (i.e., increasing the gain from the second threshold to higher-gain values) is that it was carried out adiabatically. During the return adiabatic scan a reverse symmetry-breaking (transition from symmetric to asymmetric) attractor is observed and a small region of overlap between symmetric and asymmetric solutions is identified. Figures 7(a)—7(b) show a sequence of heterodyne spectra characteristic of each region of Fig. 4. Figures 8(a) and 8(b) and 8(c) and 8(d) show typical time-dependent solutions and their respective heterodyne spectra for the asymmetric and symmetric attractors in the coexistence region. Note also in Fig. 8(b) that the central frequency is very weak in support of the notion that the asymmetric nature of the attractor "weakens" during the smooth transition into the symmetric regime.

The corresponding experimental results shown in Figs. 9(a)—9(f) for the conditions defining the numerical parameters in the previous discussion agree qualitatively with the numerical data. A quantitative one-to-one correspondence is difficult to assemble, but the sequence involving the strong asymmetric solution, the chaotic regime, and a regime where two-side frequencies are dominant, a signature of the symmetric attractor, are strong points of similarity between the numerical and experimental results. Thus, with due allowance for the complexities of the numerical and experimental systems, we find reasons to claim a fair agreement between the predictions of the model and the experimental results. The kind of details that are available from the model, of course, are partially obscured in the experiments because of unavoidable noise and other limitations on the gain levels that could be reached during our scans.

Off-resonance, both the numerical and experimental results show a greater tendency toward asymmetric patterns and a broadening of the domain of the asymmetric attractor. We must adopt a more qualitative definition of symmetric and asymmetric attractors in this case. Away from resonance, the symmetry with respect to ω_A is broken and it is unlikely that any solution will be truly symmetric in its spectrum or phase-space trajectory. However, we can still identify the frequency of the steady-state solution which is shifted now both by changes in gain (part of the mode pulling effects in inhomogeneously broadened lasers) and by the instabilities themselves. With respect to this "central" frequency component, the spectrum will be termed "asymmetric" if there is a noticeable power at that frequency and will be termed "symmetric" if there is no noticeable power at that frequency and instead there are two roughly symmetrically located peaks in the spectrum, one on either side of the central frequency.

Figure 10 shows the steady-state input intensity as a

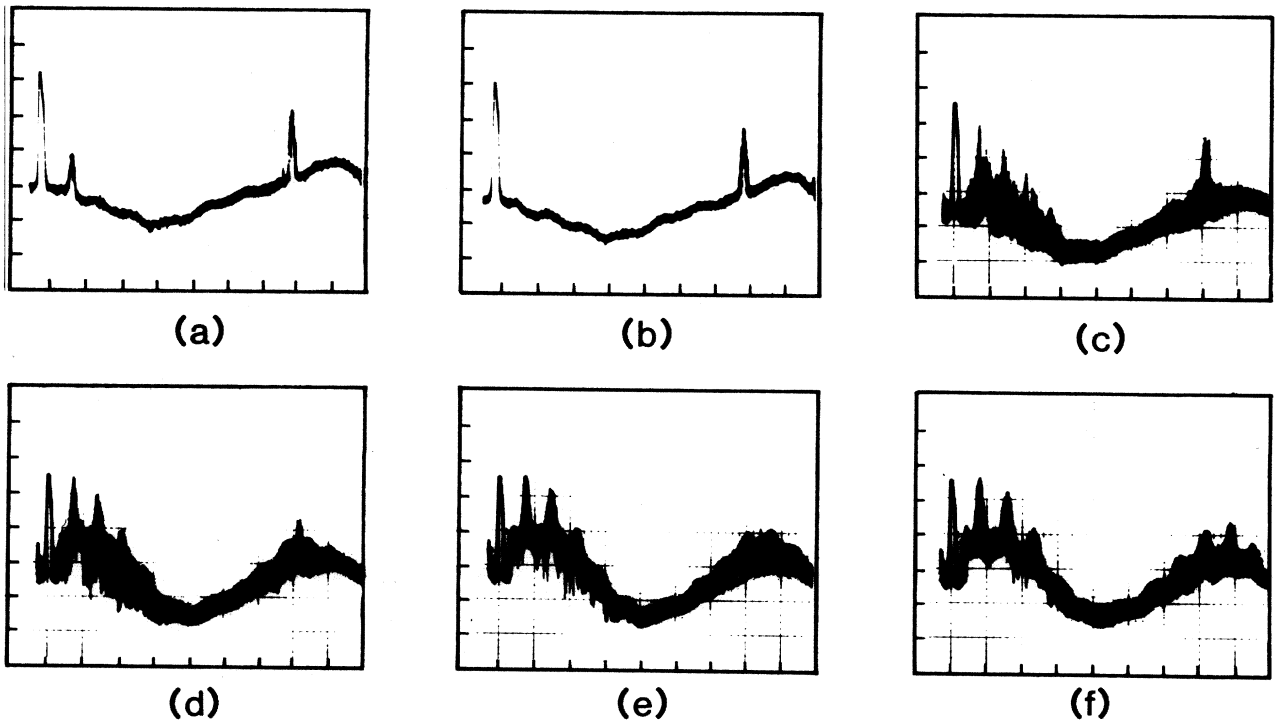

FIG. 9. Experimentally obtained homodyne and heterodyne power spectra with the laser cavity tuned to the atomic resonance for 172 mTorr of xenon-136 and 1 Torr of helium. Spectra are shown as the excitation current increases from (a) to (f). Range of the horizontal axis is from -10 to 90 MHz. Unit on the vertical axis is 10 dB. The ratios of the values of the excitation current to the value at threshold are 1.02, 1.52, 1.77, 1.89, 1.99, and 2.02, respectively. Since the laser turns off at current just above the threshold, the threshold current is extrapolated from linear low-current region of the experimental plot of the average power vs the excitation current.

function of the gain parameter C when the cavity frequency is detuned by an amount $(\frac{1}{2})\tilde{\sigma}_D$. Here the asymmetric solutions are more common in contrast with the results in the resonant scan. Other scans not shown here have also shown a similar behavior. It should be noted that the range of gain parameters in which chaos is a predominant feature diminishes with increasing detuning, suggesting a tendency for more orderly patterns. (This propensity toward order was noted in earlier theoretical studies of a detuned homogeneously broadened system, by Zeghlache and Mandel.[20])

Figures 11(a)—11(d) show the changes observed experimentally in a gain scan for a detuned case. In this figure we see that the chaotic region is absent altogether and that strong asymmetric pulsations dominate over a wide range of the gain.

Figure 12 shows the dependence of the peak frequencies of the heterodyne spectra found in numerical simulations during an adiabatic scan in the direction of increasing gain. The relative power associated with each frequency component is indicated by the size of the point, larger powers corresponding to larger points. The corresponding variation of the steady-state operating frequency of the laser is shown by a solid line. Near the instability threshold the pulsations are of small amplitude, indicated by the fact that the central peak in the pattern is the strongest. The gain-dependent mode-pulling effect is enhanced by the instability for low gains (the main laser frequency is closer to ω_A than for the corresponding steady state). This can be understood because the mode pulling in an inhomogeneously broadened laser is intensity dependent (as shown by the steady-state curve). As the pulsing solutions have large peak-intensity values and also have average in-

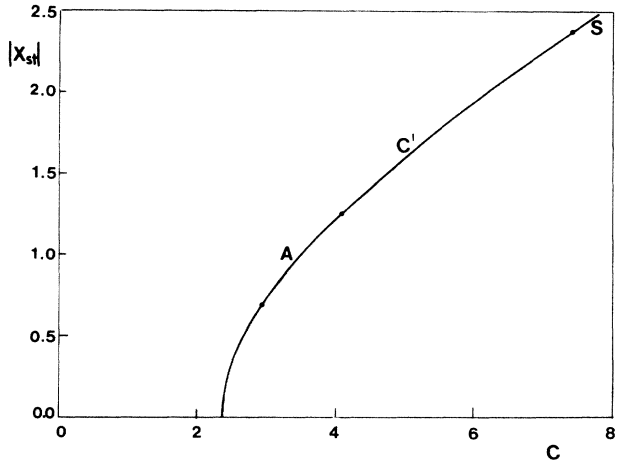

FIG. 10. Steady-state output intensity for an inhomogeneously broadened laser as a function of the gain parameter C for $\tilde{\delta}_{AC}=2.465$ and for the same parameters as in Fig. 1.

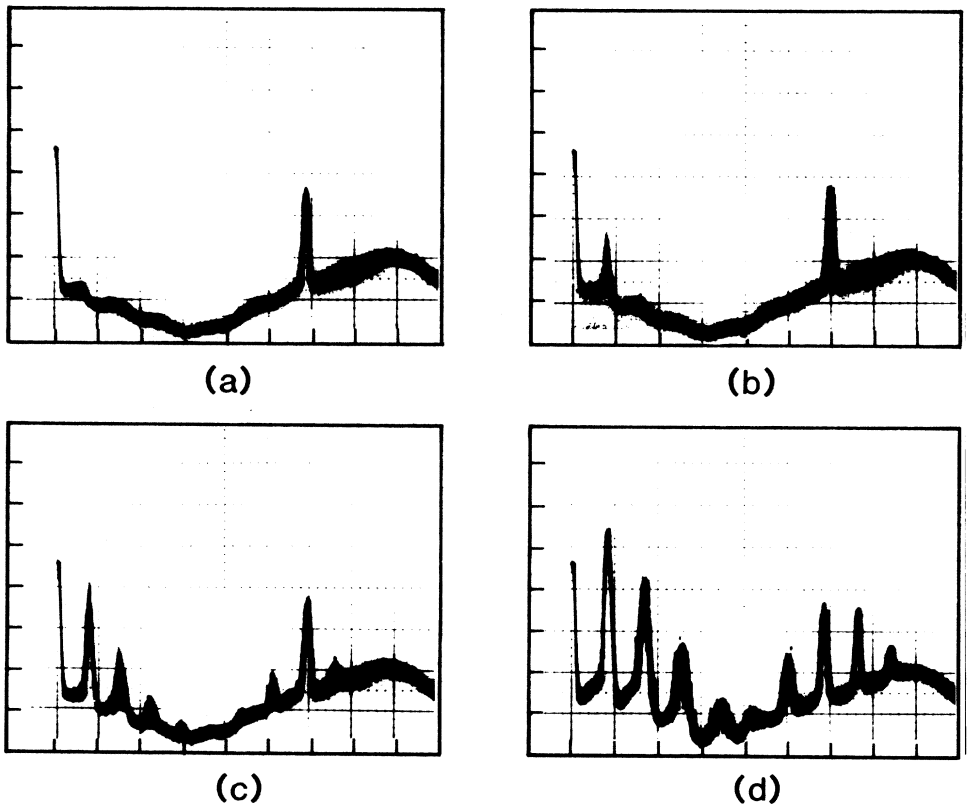

FIG. 11. Experimentally obtained homodyne and heterodyne power spectra with laser frequency detuned off-resonance by 5 MHz for 172 mTorr of xenon-136 and 1 Torr of helium. Spectra are shown as the excitation current increases from (a) to (d) for the same values of the parameters as in Fig. 1. Range of the horizontal axis is from -10 to 90 MHz. Ratios of the values of the excitation current to the value at threshold are 1.55, 1.90, 2.02, and 2.7, respectively.

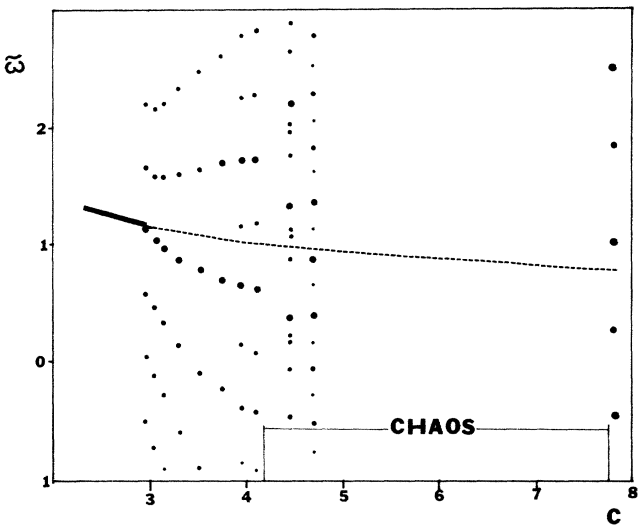

FIG. 12. Plot of the frequencies of the peaks in the numerically generated heterodyne spectra as a function of the gain parameter C for $\tilde{\delta}_{AC}=2.465$ and the same values of other parameters as in Figs. 10 and 1. For a fixed value of the gain, the larger dots indicate stronger frequencies. Solid line indicates the single frequency of the stable steady-state solutions and the dashed line indicates the frequency of the unstable steady-state solutions. Region in which broadband chaotic spectra were generally found is indicated. Several periodic windows found within the chaotic region are noted by the details of their spectra.

tensities which are larger than the intensity of the steady-state solution, it is reasonable that the mode pulling should be increased in the unstable region. However, in the periodic window above $C=4$ it appears that the center of symmetry of the spectrum is shifted further away from ω_A. In general, the heterodyne spectra in the detuned case are never symmetric about the largest peak of the approximate center of the spectrum. Thus we are unable to classify the attractors in any precise way as being symmetric or asymmetric in the phase-space plots because we cannot easily decide on a proper value of the carrier frequency before determining the slowly varying amplitudes to use in the plots. There are strong qualitative similarities to the resonant case as we see that the instabilities near threshold are similar to asymmetric attractors while in the periodic windows the attractors are nearly symmetric. Comparison of these features with the experimental data shows again qualitative agreement over the range of parameters explored in this study.

The good qualitative agreement of the numerical predictions and experimental results for the nonresonant cases is best summarized with the help of Figs. 13(a) and 13(b). These figures show the dependence of the peaks in the heterodyne spectra on the detuning under low-gain conditions for the experimental and numerical work, respectively. Both figures show that for large detunings the laser is stable giving a single optical-frequency peak. When the instability develops at large detunings the dominant laser frequency persists and is joined by weak sidebands. However, the initial dominant frequency weakens as the laser cavity is tuned into resonance and it becomes comparable in strength to one of its original sidebands which has been growing in strength. Further changes in the detuning past resonance show increasing dominance of the strengthened sideband over the original frequency.

The disagreement between our experimental and numerical results is in both the pulsing frequency and in the degree of mode pulling (the slope of the lines in the two plots). As mode pulling is affected by both changes in the gain and in the cavity losses we searched for combinations which would give better agreement. The gain could be raised slightly to achieve the same tuning range for the

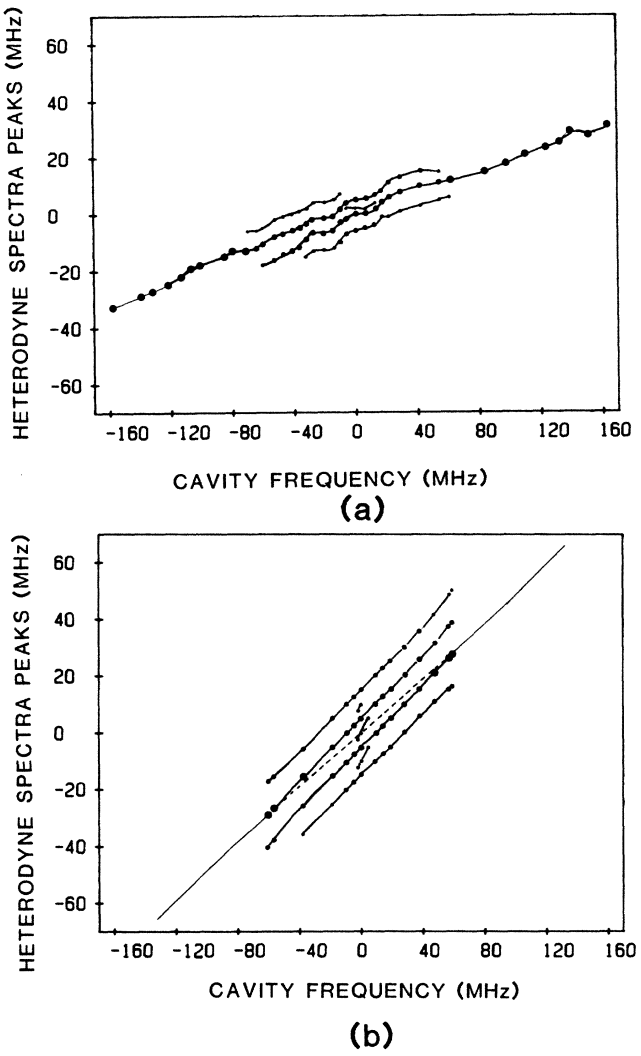

FIG. 13. (a) Plot of the experimental values of the peak frequencies in the heterodyne spectrum as a function of detuning for 175 mTorr of xenon and 667 mTorr of helium. Ratio of the value of the excitation to the value at threshold is 2.10. (b) Plot of the frequency peaks in the numerically generated heterodyne spectrum as a function of the detuning from resonance for parameters corresponding to the pressure conditions in (a). Ratio of the value of the excitation to the value at threshold at resonance is 1.26. Solid line indicates the single frequency of the stable steady-state solutions and the dashed line indicates the frequency of the unstable steady-state solutions.

laser. If the cavity loss rate $\tilde{\kappa}$ was raised, there would be larger mode pulling. Such an increase could be justified if there were additional losses in the laser which we had not specifically included in our calculations of $\tilde{\kappa}$. However, we were not able to find combinations of C and $\tilde{\kappa}$ which gave reasonably better results, suggesting that a more subtle effect may be needed for a full explanation. The differences may possibly be caused by the neglect of the velocity-induced cross-relaxation effects or by the effects of the transverse spatial dependence of the field amplitude and the gain in the experimental system. These are known to affect at least the steady states when they are included in model calculations.[11,21] Despite the quantitative differences, the qualitative features of the optical spectra are the same for both numerical and experimental detuning scans.

V. DISCUSSION AND CONCLUSIONS

We have compared experimental results from an inhomogeneously broadened single-mode Xe-He ring laser to calculations based on a MB model. We find reasonable qualitative agreement in (1) the predicted transitions from one unstable behavior to another, (2) the type of attractors that govern the dynamics of the system, and (3) the relative strength of these attractors by using spectral heterodyne techniques and phase-space portraits.

In the gain scans for the resonantly tuned case and for small values of $\tilde{\gamma}$, we observe experimentally a strong asymmetric attractor that becomes chaotic and eventually becomes two strong sidebands with a greatly weakened central frequency. This transition sequence is verified by the model calculations. Some details of the model, however, are not observed experimentally. For example, the existence of coexisting attractors, the smooth transition from one attractor to another, and the periodic windows of symmetric solutions within the chaotic regime have not been observed. On the other hand, we have been able to make contact with some of Casperson's results[10] which show that the transition regions are characterized by different types of waveforms, that an initially stable period-1 oscillation near threshold is followed by regions of chaos, and that narrow regions of periodic solutions exist within the chaotic regions. Scans for increasing gain under detuned conditions reveal that strong asymmetric solutions are more likely to persist and that there is a reduction of the role played by the dynamical chaos. Zeghlache and Mandel[20] reported a similar trend in their studies of a homogeneously broadened single-mode ring-laser model.

Also, upon changing the detuning for a fixed low value of the gain, theoretical and experimental results are found to be in good qualitative agreement. The laser operation for sufficiently large detuning is characterized by a strong central-frequency component and weak sidebands; for smaller values of the detuning, we have observed a weakening of the strong central frequency and the emergence of two symmetrically displaced peaks of approximately equal strength. Also in this range we noted the emergence of a weak central-frequency component between the two dominant symmetric peaks. Decreasing the detuning past resonance shows one of the two symmetric peaks fading in strength and the other, a formerly weak sideband, now growing in strength to dominate all other sidebands.

The detuning scan provides a more global qualitative understanding of the behavior of this inhomogeneously broadened single-mode ring laser. The domains of attraction of the symmetric and asymmetric solutions appear to be sensitive to the value of the detuning in the vicinity of resonance. The regions of chaos seem to be the result of nonlinear interactions that culminate in the competition between frequencies not clearly accessible to the system until detuning is large enough. This is rather speculative, but the idea that chaos is a result of the nonlinear interaction between the tendency to pulse with a frequency and waveform extrapolated from above the chaos region, and

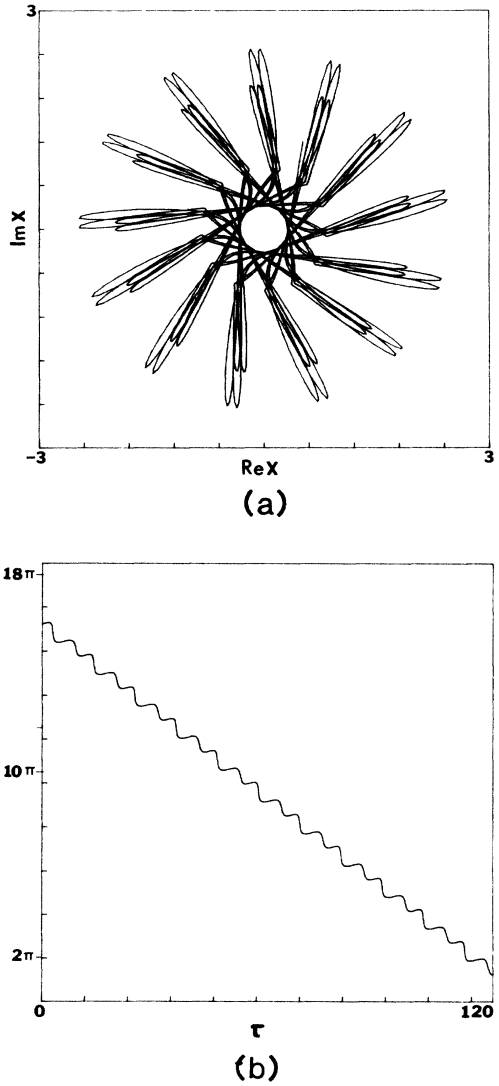

FIG. 14. (a) Phase-space portrait of ReX vs ImX for a detuned laser with $C=4.07507\ldots$ ($|X_{\rm st}|=1.25$), $\tilde{\delta}_{AC}=2.465$, $\tilde{\kappa}=6.19$, and $\tilde{\gamma}=0.243$. The gross pattern appears to rotate in the plane. (b) Plot of the phase as a function of $\tilde{\tau}=\gamma_{\perp}t$ of the solution shown in the phase-space portrait in (a). General linear trend indicates a frequency shift from the assumed reference and the kinks indicate that the phase is an active dynamical variable in the pulsations.

the tendency to pulse with an incommensurate frequency and waveform extrapolated from below the chaos region, was also conjectured by Casperson.[10] Our results provide further evidence in support of this idea.

Furthermore, the model considered here also shows that instabilities for the detuned inhomogeneously broadened laser involve dynamics of the phase of the field and polarization as well as the amplitudes of the variables. This can be seen by considering the behavior of the complex field amplitude. The slowly varying complex amplitudes of Eqs. (2.2) have time-independent (constant) amplitudes in the selected frequency reference frame (determined by the frequency selected for the optical carrier wave) only under resonantly tuned conditions. In the presence of detuning, the laser actually operates away from the assumed frequency of the carrier wave (the frequency of the steady-state solution) giving all of the "slowly varying amplitudes" a trivial oscillatory behavior at the frequency difference. If there were only this trivial frequency shift, we would conclude that the phase was not an important dynamical variable. However, the time dependence of the solution proves to be even more complicated.

A plot of a particular solution in the detuned case shows this effect as the trajectory in the projected phase space of $\mathrm{Re}X$ versus $\mathrm{Im}X$ seems to be a pattern that rotates in time as shown in Fig. 14(a). The phase of the field itself has a general linear trend in time, as shown in Fig. 14(b), the slope of which represents the frequency shift and the frequency of the rotation of the pattern in Fig. 14(a). However, there are kinks in the plot of the phase which are correlated with the intensity pulsations, indicating that the instability in the detuned case involves the phase in a dynamical way. In contrast, in the resonant case we find that the phase is quiescent after an initial evolution to an arbitrary value induced by the transient. The phase fluctuations correspond to fluctuations in the instantaneous frequency of the field. We can understand this qualitatively in the inhomogeneously broadened case because the degree of mode pulling of a steady-state solution (dispersion-induced frequency shifts) strongly depends on the degree of saturation of the medium. In the pulsed state there are pulsations in all of the coupled variables so that one cannot speak of an equilibrium dispersion, but it seems plausible that the fluctuations include dispersion fluctuations that cause the pulsations in the frequency of the laser operation.

Finally, we note some strong similarities between the results of our study and similar analyses carried out on the homogeneously broadened single-mode laser for small values of $\bar{\gamma}$.[7] These similarities are also found in the corresponding experiments.[22] Most notable in all existing studies on resonance is the tendency to evolve with strong pumping toward strong symmetric attractors with characteristic "bichromatic" spectra. Also, all cases show that detuning tends to reduce the chaotic behavior. It is surprising that homogeneously and inhomogeneously broadened systems should display so many similarities even though the instability thresholds are very different and even though it has been suggested that there are distinctly different dynamical origins for the instabilities in the two cases. Nevertheless, the preliminary evidence indicates there are several common features associated with unstable laser operation that are independent of the nature of the type of broadening of the atomic resonance.

ACKNOWLEDGMENTS

We are grateful to Dr. J. R. Tredicce for many stimulating discussions. The support and encouragement of R. S. Gioggia in our experimental work was also invaluable. This work was supported in part by a grant from the National Science Foundation, No. ECS-8210263, and by a contract with the Army Research Office, No. 22919-PH. M.F.H.T. acknowledges the support of the Newport Research Corporation through the Optical Society of America. D.K.B. acknowledges the support of the Helen Schaffer Huff Fund of Bryn Mawr College for a portion of this work.

[1]A. V. Uspenskii, Radiotekh. Electron. **8**, 1165 (1963) [Rad. Eng. Electron. Phys. (USSR) **8**, 1145 (1963)]; V. V. Korobkin and A. V. Uspenskii, Zh. Eksp. Teor. Fiz. **45**, 1003 (1963) [Sov. Phys.—JETP **18**, 693 (1964)]; A. Z. Graysiuk and A. N. Oraevskii, Radiotekh. Electron. **9**, 524 (1964) [Rad. Eng. Electron. Phys. (USSR) **9**, 424 (1964)]; in *Quantum Electronics and Coherent Light,* edited by P. A. Miles (Academic, New York, 1964), p. 192.

[2](a) H. Haken, Z. Phys. **190**, 327 (1966); see also (b) H. Haken, Phys. Lett. **53A**, 77 (1975).

[3]H. Risken and K. Nummedal, J. Appl. Phys. **39**, 4662 (1968); R. Graham and H. Haken, Z. Phys. **213**, 420 (1968).

[4]N. B. Abraham, L. A. Lugiato, and L. M. Narducci, J. Opt. Soc. Am. B **2**, 7 (1985).

[5]L. A. Lugiato and M. Milani, Z. Phys. B **50**, 171 (1985).

[6]W. Klische and C. O. Weiss, Phys. Rev. A **31**, 4049 (1985).

[7]L. M. Narducci, H. Sadiky, L. A. Lugiato, and N. B. Abraham, Opt. Commun. **55**, 370 (1985).

[8]U. S. Idiatulin and A. V. Uspenskii, Radiotekh. Electron. **18**, 580 (1973) [Rad. Eng. Electron. Phys. (USSR) **18**, 422 (1973)].

[9]L. W. Casperson, IEEE J. Quantum. Electron. QE-**14**, 756 (1978).

[10]L. W. Casperson, J. Opt. Soc. Am. B **2**, 62 (1985).

[11]L. W. Casperson, J. Opt. Soc. Am. B **2**, 73 (1985).

[12]J. Bentley and N. B. Abraham, Opt. Commun. **41**, 52 (1982).

[13]N. B. Abraham, T. Chyba, M. Coleman, R. S. Gioggia, N. J. Halas, L. M. Hoffer, S. N. Liu, M. Maeda, and J. C. Wesson, *Laser Physics,* Vol. 182 of Lecture Notes in Physics, edited by J. D. Harvey and D. F. Walls (Springer-Verlag, Berlin, 1983), p. 107.

[14]See Refs. 9—11; S. T. Hendow and M. Sargent III, J. Opt. Soc. Am. B **2**, 84 (1985); M. Minden and L. W. Casperson, *ibid.* **2**, 120 (1985); M. L. Shih, P. W. Milonni, and J. R. Ackerhalt, *ibid.* **2**, 130 (1985).

[15]L. A. Lugiato, L. M. Narducci, D. K. Bandy, and N. B. Abraham, Opt. Commun. **46**, 115 (1983).

[16]D. K. Bandy, L. M. Narducci, L. A. Lugiato, and N. B. Abraham, J. Opt. Soc. Am. B **2**, 56 (1985).

[17]ω_L is identified with the carrier frequency of the steady-state solution of the laser equations [see, for example, Ref. 16, Eqs. (2.12)] even when this solution is unstable.

[18]N. B. Abraham, L. A. Lugiato, P. Mandel, L. M. Narducci, and D. K. Bandy, J. Opt. Soc. Am. B **2**, 35 (1985).

[19]L. M. Narducci, J. R. Tredicce, L. A. Lugiato, N. B. Abraham, and D. K. Bandy, Phys. Rev. A **33**, 1842 (1986); J. R. Tredicce, L. M. Narducci, N. B. Abraham, D. K. Bandy, and L. A. Lugiato, Opt. Commun. **56**, 435 (1986).

[20]H. Zeghlache and P. Mandel, J. Opt. Soc. Am. B **2**, 18 (1985).

[21]L. W. Casperson and A. Yariv, Appl. Opt. **11**, 18 (1972).

[22]W. Klische, C. O. Weiss, W. Al-Soufi, and G. Huttman, *Optical Instabilities,* edited by R. W. Boyd, M. G. Raymer, and L. M. Narducci (Cambridge University Press, London, 1986), p. 237; E. H. M. Hogenboom, W. Klische, C. O. Weiss, and A. Godone, Phys. Rev. Lett. **55**, 2571 (1985).